Journal of Hydrology: Regional Studies 66 (2026) 103718

Contents lists available at ScienceDirect

Journal of Hydrology: Regional Studies

journal homepage: www.elsevier.com/locate/ejrh

Estimation of extreme rainfall using intensity-duration-frequency curves for Ashanti Region, Ghana

G.A. Torsah[a,*], M. Maranan[b], V. Akyeampong[c], K.A. Adjei[c], L.K. Amekudzi[a], A. H. Fink[b]

[a] Kwame Nkrumah University of Science and Technology (KNUST), College of Science, Department of Meteorology and Climate Science, Kumasi, Ghana

[b] Institute of Meteorology and Climate Research, Karlsruhe Institute of Technology, KIT, Karlsruhe, Germany

[c] Kwame Nkrumah University of Science and Technology, KNUST; College of Engineering, Department of Civil Engineering, Kumasi, Ghana

ARTICLE INFO

Keywords:
GEV Distributions
IDF curves
Extreme rainfall
Concatenation
Disaggregation
Ashanti Region

ABSTRACT

This study addresses the challenge of constructing Intensity-Duration-Frequency (IDF) curves in Ghana's Ashanti Region, where sparse gauge networks limit high-resolution extreme rainfall analysis. A 36-station-year annual maximum series (AMS) was developed by concatenating 14 sub-daily stations from the Kumasi Meso Rain Gauge Network (KMRGN), creating a continuous regional reference series. The validity of this concatenation approach was supported by L-moment-based regional frequency analysis, confirming statistical homogeneity of the network despite localized variability in higher-order moments. Temporal consistency analysis further indicates no statistically significant trends or change-points in the AMS, supporting the assumption of stationarity for extreme-value modelling. The AMS of the benchmark concatenated sub-daily series is modeled within a Generalized Extreme Value (GEV) framework, complemented by intercomparison with Gumbel, Pearson Type III, and Log-Pearson Type III distributions under a multi-criteria model selection approach. The distributions of each model are validated using Chi-square and Kolmogorov-Smirnov tests, and are applied to construct and compare IDF curves. Results from the multi-criteria framework indicate that the Log-Pearson Type III distribution provides the most balanced performance in terms of goodness-of-fit, bias, and stability of extreme estimates. This benchmark is used to evaluate AMS derived from disaggregated daily records from the Ghana Meteorological Agency network. Results show that the concatenated sub-daily AMS reliably captures short-duration rainfall intensities while atte station-specific anomalies. However, disaggregated daily AMS underestimated short-duration (12 min-1 h) intensities by up to −18%, particularly during the convectively active minor rainy season, reflecting smoothening of peak rainfall. Performance improves at longer durations, and when concatenated into a 220 station-year homogeneous regional series, the disaggregated data closely reproduce the regional intensity structure across durations and return periods. Uncertainty analysis reveals strong duration dependence, with the highest sensitivity at short durations primarily controlled by the nonlinear scaling exponent of the disaggregation procedure. Comparison of disaggregated curves with existing 2016 IDF curves from the Ghana Meteorological Agency under the Gumbel distribution, similarly adopted by the agency, indicates systematic positive biases, ranging 20–40% on

* Corresponding author.
E-mail addresses: godfredtorsah2808@gmail.com, godfred.torsah@knust.edu.gh (G.A. Torsah), marlon.maranan@kit.edu (M. Maranan), vidaakye@gmail.com (V. Akyeampong), nanakadjei@gmail.com (K.A. Adjei), leonard.amekudzi@gmail.com (L.K. Amekudzi), andreas.fink@kit.edu (A.H. Fink).

https://doi.org/10.1016/j.ejrh.2026.103718
Received 3 March 2026; Received in revised form 2 July 2026; Accepted 3 July 2026
Available online 10 July 2026

average across all durations for each return period and more than 50% increase in rainfall intensity at longer return periods across the respective durations and return periods, suggesting intensification of extremes. However, the absence of statistically significant trends in the AMS suggests that these increases are largely attributable to extended sampling, improved temporal representation, and methodological differences rather than definitive climatic non-stationarity. These findings establish the concatenated sub-daily series as a robust regional reference and highlight the necessity of high-resolution data or seasonally adjusted correction methods for reliable flood risk assessment, infrastructure design, and climate adaptation planning in the region.

1. Introduction

The design of stormwater management and drainage systems, including dams, remains a fundamental component of urban and regional planning (Niemczynowicz, 1999). These systems are critical for mitigating flood-related risks and safeguarding life and property (Ansah et al., 2020). A central tool in this process is the intensity-duration-frequency (IDF) curve, which describes the relationship between rainfall intensity, duration, and frequency of extreme events (Claude et al., 2021). IDF relationships provide the quantitative basis for hydraulic design standards and flood risk assessment (Chow, 1988). Rapid urbanization and population growth have further intensified the need for reliable estimation of design rainfall (Amoateng et al., 2018).

In tropical regions, particularly across West Africa, rainfall extremes are dominated by convective systems and mesoscale processes that exhibit strong spatial and temporal variability (Nicholson, 2013). These characteristics lead to short-duration, high-intensity rainfall events that are often responsible for flash flooding. Accurate representation of such extremes requires high-resolution rainfall observations, as daily datasets are unable to resolve the intermittency and peak intensities associated with convective storms (Westra et al., 2014). However, across Southern West Africa, the availability of long-term sub-daily rainfall data remains limited, posing a major constraint for hydrological design and risk assessment (Amekudzi et al., 2016; Maranan et al., 2018).

In Ghana, these challenges are particularly pronounced in that most available rainfall records are at daily resolution, and even these are often characterized by gaps and inconsistencies (GMet, 2016). Historically, IDF curves in Ghana were first developed using daily rainfall data (Dankwa, 1974) and later updated using similar datasets combined with statistical modelling approaches (GMet, 2016). While these efforts provided important national benchmarks, they inherently lack direct representation of sub-daily rainfall dynamics critical for engineering design. To address this limitation, several studies have applied empirical disaggregation techniques, such as the Indian Meteorological Department (IMD) reduction formula, to derive sub-daily rainfall from daily totals (Asante-Annor and Oti, 2019). Although useful, such approaches introduce structural uncertainties and tend to smooth peak intensities, particularly for convective rainfall (Sam et al., 2021). This limitation is well established, as temporal disaggregation often fails to reproduce the intermittency and peak structure of short-duration extremes (Olsson, 1998; Cannon and Innocenti, 2019). Other efforts (e.g., Fordjour et al., 2019) have attempted to construct IDF curves using sub-daily durations; however, these are constrained by data availability and potential inconsistencies in high-resolution observations. Thus, generally, the lack of long-term, high-resolution rainfall records remains a critical limitation in the development of robust IDF relationships in Ghana.

Within this national context, the Ashanti Region represents a critical case study where rapid urbanization, complex drainage characteristics, and frequent flood events converge (Owusu-Ansah, 2016; Amoateng et al., 2018). Flooding in the region is influenced not only by rainfall extremes but also by land-use practices, wetland encroachment, and limitations in drainage infrastructure (Campion and Venzke, 2013). While these anthropogenic factors exacerbate flood impacts, the reliability of underlying rainfall design estimates remains a fundamental constraint in effective flood management.

To address the limitations of daily rainfall data, recent observational initiatives have provided new opportunities for high-resolution analysis. The Kumasi Meso Rain Gauge Network (KMRGN), established under the DACCIWA and FURIFLOOD projects, provides 1-minute rainfall observations across the Ashanti Region from 2015 to 2023 (Maranan et al., 2020). These data enable direct characterization of sub-daily rainfall variability, including convective storm initiation, peak intensity, and temporal evolution, which are not captured in conventional daily datasets. Previous studies have demonstrated the value of KMRGN data for analyzing extreme rainfall dynamics, diurnal variability, and satellite validation in the region (Torsah et al., 2025).

However, the relatively short duration of these high-resolution records limits their direct application for frequency analysis, which typically requires multi-decadal datasets. To overcome this constraint, this study adopts a concatenation-based regionalization approach, in which multiple high-quality station records are combined under the assumption of regional homogeneity to extend the effective record length. This approach is conceptually consistent with regional frequency analysis (RFA), which pools information across sites to improve estimation of extreme quantiles (Hosking and Wallis, 1997; Estrany-Planas et al., 2025), but is adapted here to address the scarcity of continuous sub-daily observations.

Motivated by these challenges, this study addresses the following research questions: (i) How can short-duration rainfall extremes be robustly characterized in a data-scarce environment? (ii) To what extent can high-resolution sub-daily observations improve IDF estimation relative to disaggregated daily datasets? (iii) How reliable is the concatenation-based regionalization approach as a surrogate for long-term high-resolution records? To address these questions, IDF curves are derived using the concatenated KMRGN dataset and evaluated against disaggregated daily rainfall records. The findings are intended to support improved flood-risk assessment and infrastructure design in the Ashanti Region. The remainder of the paper is organized as follows: Section 2 describes the study area, data, and method in Section 3; results and discussion in Section 4; and finally, conclusions in Section 5.

2. Study area

The Ashanti Region, located in the moist semi-deciduous forest zone of southern Ghana on the Guinea Coast of West Africa (Asubonteng and Andah, 2001), is the second-largest administrative region among the sixteen regions in Ghana (Mensah et al., 2021). The land area of the region is approximately 24,389 km^2. It is bounded between longitude 2.5 ° W- 0.5 ° W and latitude 5.5 ° N- 6.7 ° N with a population of more than four million according to the 2021 Population and Housing Census (https://census2021.statsghana.gov.gh/).

The region is characterized by a heterogeneous landscape, comprising low-lying plains, rolling hills, and upland areas. Elevation ranges from ≈ 26–790 m above the mean sea level (MSL), with the central and eastern portions exhibiting moderate relief, whilst the western and northern zones feature significant upland terrain and escarpments. The regional capital, Kumasi, is centrally located within this topographical gradient and lies 250–300 m above MSL. Varied elevations influence local climate dynamics, contributing to the spatial heterogeneity of rainfall in the region. The region falls under the equatorial climate belt, characterized by a bimodal rainfall regime, with a major rainy season from March to July and a minor season from September to November (Amekudzi et al., 2015). The seasonal rainfall pattern is largely modulated by the latitudinal migration of the Inter-Tropical Discontinuity (ITD), and the dynamics of the Azores and St. Helena high-pressure systems (Ansah et al., 2020). During the wet season, the intensification of the St. Helena High induces the advection of southwesterly maritime air masses from the Gulf of Guinea, while the dry season is dominated by the incursion of northeasterly continental air masses, driven by the Azores High, resulting in dry and dusty Harmattan conditions. The distribution of rain gauge stations across the region, as shown in Fig. 1, reflects a comprehensive integration of observational data sources to enhance the spatial and temporal resolution of rainfall characterization. Over the years, the region has experienced notable climatic anomalies such as the severe droughts of 1982, 1983, and 1994, which had widespread socio-economic impacts, including food insecurity, wildfires, and loss of agricultural productivity (Adjei-Mensah and Kusimi, 2020; Asibey et al., 2020).

2.1. Data and methods

The study employed high temporal resolution rainfall data from optical rain gauges established in the framework of the Dynamics-Aerosol-Chemistry-Cloud Interactions in West Africa (DACCIWA; 2013–2018) and Current and Future Risks of Urban and Rural Flooding in West Africa (FURIFLOOD; 2021–2024) projects, along with daily rainfall data from the Ghana Meteorological Agency

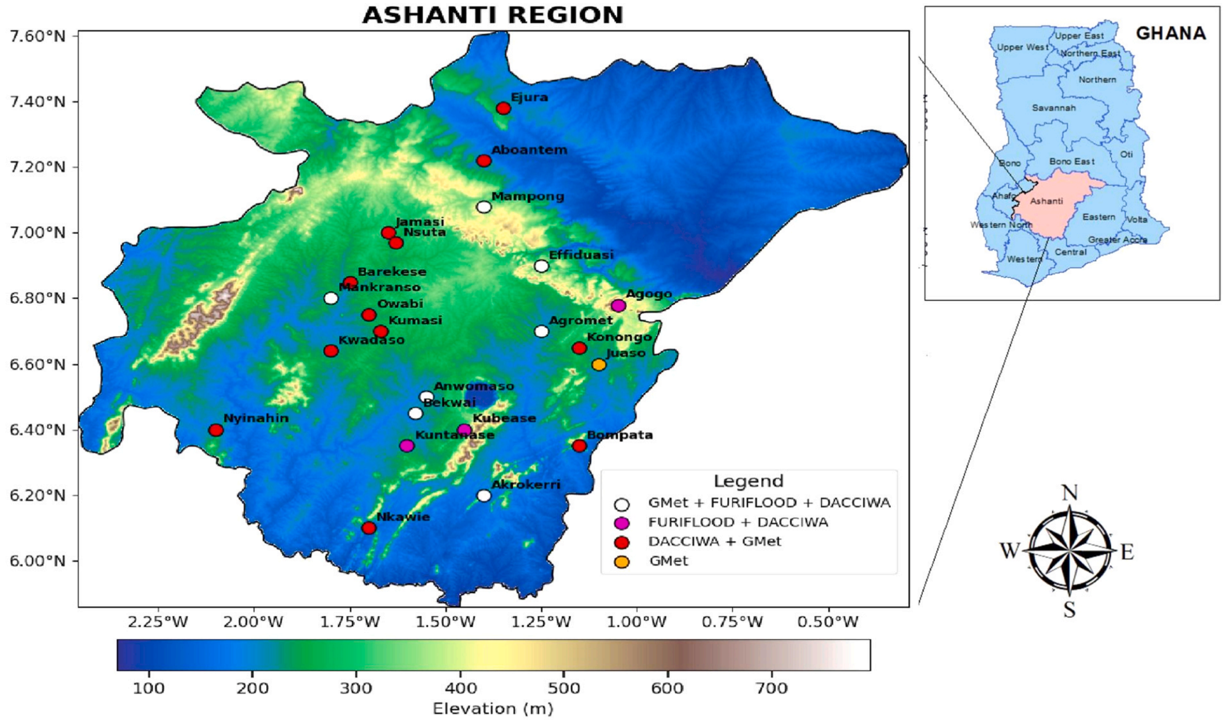

Fig. 1. Map of Ashanti Region showing the spatial distribution of rainfall stations from multiple instruments, which include GMet, and those from the DACCIWA and FURIFLOOD projects. The colored markers indicate station types: white dots denote all three gauges (GMet, DACCIWA, and FURIFLOOD), magenta denotes DACCIWA and FURIFLOOD, and a red dot denotes DACCIWA and GMet, and yellow dots denote GMet only. The background of the Ashanti Region displays a Digital Elevation Model (DEM) with elevation values ranging from 26 m to 790 m.

(GMet). The initial DACCIWA network, installed across Ghana's Ashanti Region in 2015, comprised 17 rain gauges that captured rainfall at 1-minute resolution by detecting and counting individual raindrops. Due to material degradation over time, the FURIFLOOD project reactivated 10 of the original DACCIWA gauges from 2022 onwards.

The high temporal resolution of the DACCIWA and FURIFLOOD datasets, constituting the KMRGN, provide detailed minute-by-minute rainfall information, offering advantages over daily GMet estimates for studying extreme rainfall and flash-flood dynamics in the region (Maranan et al., 2020; Agyekum et al., 2023). The FURIFLOOD project reactivated and upgraded ten of the DACCIWA gauges to complement existing GMet stations in and around Kumasi, Ghana. These gauges cover an area of approximately 4338 km^2 at elevations ranging from 250 to over 350 m MSL and are suitable for monitoring extreme rainfall events and conducting sub-hourly analyses of daily rainfall extremes.

GMet Standard Rain Gauge (SRG) measurements provide daily rainfall data across surface stations in the Ashanti Region. Ten of these highly quality-controlled stations have data available from the Karlsruhe Institute of Technology African Surface Stations Database (KASS-D) spanning 1980–2023 (Ageet et al., 2022). Despite limitations such as sparse coverage and measurement errors (Westra et al., 2014), surface rain gauge observations remain critical for providing direct and accurate estimates of daily and sub-daily rainfall extremes and variability.

2.1.1. Kumasi Meso Rain Gauge network and data availability

The KMRGN comprises 17 DACCIWA stations, later continued by 10 FURIFLOOD automatic surface rain gauges distributed across the Ashanti Region (Fig. 2). Station records span 2015–2023; however, record length and data completeness vary substantially across stations and years. Data completeness was quantified at 1-minute resolution and expressed as the percentage (%) of expected observations within each calendar year and season. Completeness was evaluated for (i) the full year ("All"), (ii) the major rainy season (March-July), and (iii) the minor rainy season (September-November). Across the network, completeness ranges from approximately 0–100%, with pronounced data gaps emerging after 2020 for several stations. Missing periods were retained as observed, and no arbitrary infilling was performed. Only station-year combinations with $\leq$ 10% missing data (i.e., $\geq$90% completeness) were retained for annual and seasonal extreme rainfall analyses. Screening was conducted independently for each station and season to preserve station-specific data integrity. This implies that certain years satisfy the numerical completeness threshold for the major rainy season but are followed by near-complete data loss during the minor season, rendering them unsuitable for minor season and annual analyses. Such years include 2021 for Akrokerri, Bompata, Effiduasi, Kuntanase, Mampong, Nsuta, and Nyinahin. Moreover, Kuntanase fails to meet the $\geq$ 90% completeness criterion for both seasons and was therefore excluded completely. This seasonal discontinuity explains the pronounced gaps observed after 2021. Although ten of the DACCIWA stations were continued during the FURIFLOOD project from

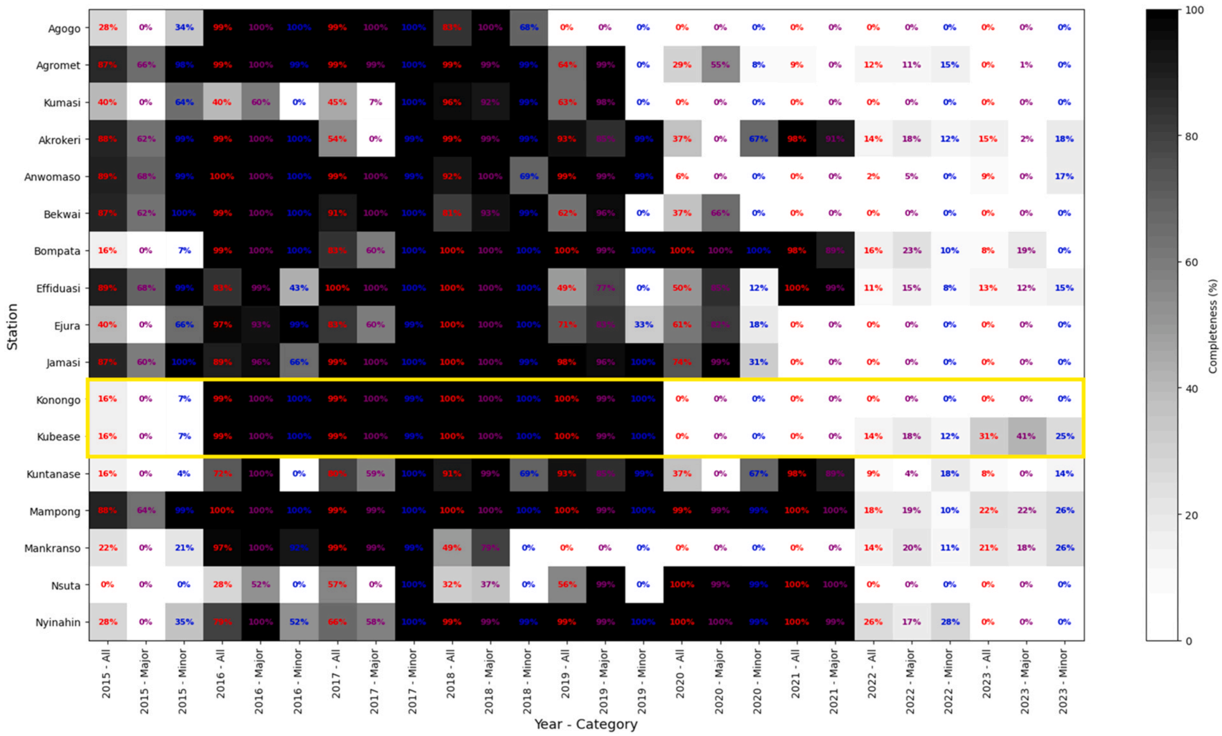

Fig. 2. Yearly and seasonal data availability for each station, expressed as a percentage (%) of the expected recording period. Stations highlighted with a yellow bounding box (Konongo and Kubease) were excluded from the IDF analysis due to systematic data duplication, as their annual maxima were identical across all years of record, indicating telemetry or recording errors. Refer to the text for more details.

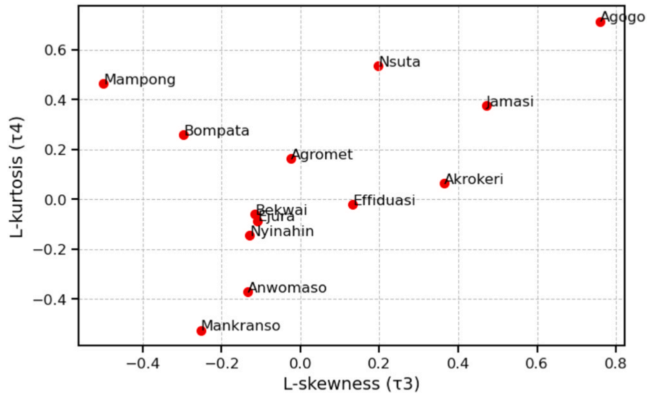

Fig. 3. L-moment ratio diagram showing the relationship between L-skewness (τ_3) and L-kurtosis (τ_4) for all stations in the KMRGN. The clustering behavior of the stations supports the suitability of regional frequency analysis, the homogeneity assumption, and the identification of discordant stations.

2022 onwards, no improvement in data estimation was observed. Quality control further identified systematic errors at two stations, Konongo and Kubease. For the period 2015–2019, their sub-daily annual maxima were identical across all years. Aggregating the 1-minute data to daily totals yielded a similar pattern of annual maxima. Despite the closeness of these stations, the exact correspondence in annual maxima between two separate stations over a range of years is physically implausible and indicates systematic data duplication or telemetry error. Cross-referencing with GMet daily station records revealed no available daily data for these stations during this period, and gridded satellite-based estimates (IMERG (Integrated Multi-satellitE Retrievals for the Global Precipitation Measurement) and CHIRPS (Climate Hazards Group InfraRed Precipitation with Station data)) showed no extreme signals on the affected dates. Consequently, both stations were excluded from the IDF analysis. While the exclusion of these stations may lead to conservative underestimation of upper-tail quantiles, retaining these demonstrably erroneous records would introduce a more severe non-physical bias. The yellow bounding box highlights the excluded stations in Fig. 2. For seasonal analysis, the major and minor rainy seasons were extracted independently from each station record prior to concatenation to ensure that seasonal statistics and extreme rainfall characteristics reflect local rainfall behaviour. Thus, a total of 14 stations exhibiting consistent completeness ($\geq$90%) across both annual and seasonal categories were subsequently concatenated to extend the effective record length required for robust IDF analysis, yielding a total of 36 station-year series of 1-minute data.

In this study, concatenation refers to the sequential pooling of valid station-year records into a composite regional series, rather than the merging of simultaneous observations. Each station-year satisfying the $\geq$ 90% completeness criterion is treated as an approximately independent realization of the same homogeneous rainfall process and appended end-to-end, yielding 36 pooled station-years rather than a continuous 36-year record at one location. This follows the logic of station-year pooling in regional frequency analysis, where observations from homogeneous sites are treated as approximately independent samples (Leadbetter, 1974; Hosking and Wallis, 1997; Estrany-Planas et al., 2025). Although some inter-station dependence may occur during widespread convective events, the annual block-maxima framework reduces its influence because only one maximum per station-year is retained; residual dependence mainly affects uncertainty rather than central return-level estimates (Coles, 2001; Koutsoyiannis, 2004). No averaging or spatial smoothing is applied, so rainfall extremes remain in their original magnitude.

The concatenation assumes that KMRGN stations lie within a climatologically homogeneous region, such that short-duration rainfall extremes share comparable statistical properties across the network, an assumption supported by the small spatial separation of stations and broadly consistent seasonal rainfall characteristics across the Ashanti Region. This assumption is formally evaluated in Section 2.1.2 using an L-moment-based regional homogeneity assessment (Hosking and Wallis, 1997), providing quantitative support for the validity of pooling station-year records.

2.1.2. Regional homogeneity assessment based on L-moment method

The concatenation approach assumes that the selected KMRGN stations form a sufficiently homogeneous region for pooling extreme rainfall information. This assumption was evaluated using an L-moment-based regional frequency analysis following Hosking and Wallis (1997). Because the strict $\leq$ 10% missing-data criterion left too few years for stable station-level L-moment estimation, a relaxed $\leq$ 30% threshold was used only for this diagnostic assessment. For each station, L-mean, L-CV, L-skewness, and L-kurtosis were computed from the annual maximum series and evaluated using discordancy and heterogeneity measures.

All stations satisfied the discordancy criterion, with Di values below the critical threshold of 3. The Hosking-Wallis heterogeneity statistic was H = 0.080 for the sub-daily KMRGN AMS, classifying the network as homogeneous. The same analysis applied to the daily AMS dataset gave H = 0.152, also indicating regional homogeneity. These results support the use of pooled station-year information for regional IDF estimation (for detailed methodology, refer to Estrany-Planas et al., 2025).

The assessment is not interpreted as evidence that all stations have identical rainfall distributions. Some dispersion in higher-order L-moment ratios remains, particularly for sub-daily extremes, reflecting localized variability in convective rainfall. However, the level of variability is sufficiently small not to invalidate regional pooling. Full station-level L-moment statistics and discordancy measures are provided in Supplementary Table S1.

2.1.3. Temporal consistency of AMS of the concatenated KMRGN and the individual daily stations

The suitability of the AMS for stationary frequency analysis was evaluated using trend and change-point tests. The non-parametric Mann-Kendall test and Sen's slope estimator were used to assess monotonic trends, while the Pettitt, Buishand range, and Standard Normal Homogeneity Test were applied to identify abrupt shifts in the mean structure. These tests were applied to the concatenated KMRGN AMS and to the individual daily station AMS series.

For the concatenated KMRGN AMS, the Mann-Kendall test indicated no statistically significant trend at the 5% level ($p = 0.095$), although a weak positive tendency was observed ($\tau = 0.21$; Sen's slope ≈ 0.017). Change-point analysis also provided no consistent evidence of structural inhomogeneity: the Pettitt test suggested a possible but non-significant shift ($p = 0.086$), while the Buishand and SNHT tests showed no evidence of a break ($p = 0.832$ and $p = 0.958$, respectively). The individual daily stations showed the same general pattern, with no statistically significant trends or change points detected.

These results indicate that the AMS is statistically compatible with the stationarity assumption over the available record. Accordingly, a stationary extreme-value framework was adopted for IDF estimation. Full station-level test results are provided in Supplementary Table S2.

2.2. Modeling extrema of random processes

Generally, there are two main approaches to identifying and modeling the extrema of a random process: the Block Maxima Approach (BMA) and the Peak-Over-Threshold (POT) method. In the BMA, the maxima extracted from non-overlapping blocks of observations are assumed to follow a Generalized Extreme Value (GEV) distribution (Gumbel, 1958), and the POT method fits exceedances over a high threshold to a Generalized Pareto Distribution (GPD) (Pickands, 1975). The BMA is often preferred when data are recorded over long, consistent time periods, whereas the POT method provides more flexibility when dealing with shorter records or when multiple exceedances per year are relevant (Coles et al., 2001).

In this study, the BMA is employed to extract the Annual Maximum Series (AMS) of the rainfall data. The success of this approach has been demonstrated in several studies analyzing extreme rainfall in West Africa (Panthou et al., 2012, 2014; Osei et al., 2021). Leadbetter (1974) asserted that GEV models require datasets that are identically and independently distributed (i.i.d.) or exhibit only short-term dependence.

Let the variables $X_1,\ldots,X_m$ be a sequence of m *i.i.d.* random variables representing rainfall intensities and $x_1,\ldots,x_m$ their observed realizations. With BMA, we divide the series into blocks of n observations, from which the maximum value is extracted for each block. This yields a vector of $N = m / n$ maxima z, representing N realizations of the block maxima variable Z:

$$z = \{z_1,\ldots,z_n\} = \{\max(x_1,\ldots,x_n), \max(x_{n+1},\ldots,x_{2n}),\ldots,\max(x_{k-n+1},\ldots,x_k)\}.$$

In this study, each block corresponds to one calendar year ($n = 365$ observations). If $X_1,\ldots,X_k$ are i.i.d., then the resulting block maxima $Z_1,\ldots,Z_N$ form an approximately i.i.d. sample from the block-maxima distribution Z.

The cumulative distribution function (CDF) of the GEV distribution is given by:

$$F(x) = exp\left\{ -\left[1 + \xi\left(\frac{x-\mu}{\sigma}\right)\right]^{-\frac{1}{\xi}} \right\} \tag{1}$$

where μ is the location parameter, $\sigma > 0$ *is* the scale parameter, and ξ *is* the shape parameter. The shape parameter describes the tail behaviour: positive ξ corresponds to a heavy-tailed (Fréchet) distribution, negative ξ to a bounded (Weibull) distribution, and $\xi = 0$ yields the Gumbel (light-tailed) distribution (Gumbel, 1958):

$$G(x;\ \sigma,\ \mu) \ = \ exp\left\{ -exp\left(-\left(\frac{x-\mu}{\sigma}\right) \right) \right\} \tag{2}$$

.

Although the Gumbel distribution has been widely applied in rainfall frequency analysis, it is a restricted form of the Generalized Extreme Value (GEV) distribution obtained when the shape parameter $\xi = 0$. In this study, the GEV model was fitted using both maximum likelihood and L-moment methods to evaluate the validity of this restriction.

2.2.1. BMA-GEV parameter estimation

GEV parameters were estimated using both maximum likelihood estimation (MLE) and the method of L-moments to assess parameter stability, particularly for the shape parameter ξ, which controls tail behaviour and is sensitive to sample size and extreme observations. The comparison indicates that ξ varies across stations and estimation methods, with some estimates close to zero while others depart from the Gumbel assumption. This suggests that fixing $\xi = 0$ is not universally supported by the data.

For the concatenated KMRGN AMS, MLE and L-moment estimates showed broadly consistent signs and magnitudes, supporting the use of GEV as a flexible reference model in the distribution comparison. Given the limited sample size of the concatenated KMRGN AMS and the robustness of L-moments for regional frequency analysis, L-moment estimates were used for GEV parameter estimation in the main analysis. MLE was retained only where required for consistency with the existing GMet IDF comparison. Full station-level parameter estimates are provided in Supplementary Table S3.

2.3. Frequency distribution and IDF curves construction

Extreme rainfall quantiles were estimated by fitting candidate probability distributions to the AMS for each duration. The Gumbel distribution was considered as a special case of the Generalized Extreme Value (GEV) distribution with zero shape parameter (ξ=0), while the full GEV model allows flexible tail behaviour through non-zero ξ. For a return period T, the rainfall depth P was obtained from the fitted quantile function using the non-exceedance probability F= 1 −1/T. For the GEV distribution,

$$P_T = \mu + \frac{\sigma}{\xi}\left(\left[-\ln\left(1-\frac{1}{T}\right)^{-\xi}\right]-1\right), \quad \xi \neq 0 \tag{3}$$

where μ, σ, and ξ are the location, scale, and shape parameters, respectively. For ξ= 0, the GEV reduces to the Gumbel distribution:

Rainfall intensity was then calculated as:

$$I_T = \frac{P_T}{T_d} \tag{4}$$

.

To avoid reliance on a single distribution, four candidate models were evaluated: GEV, Gumbel, Pearson Type III, and Log-Pearson Type III. These distributions were selected because they are widely used in rainfall and flood frequency analysis and represent different assumptions about skewness and tail behaviour. Model performance was assessed using a multi-criteria framework combining goodness-of-fit, ensemble-relative deviation, and upper-tail stability. Goodness of fit was evaluated using Kolmogorov-Smirnov and Chi-square tests. Ensemble-relative deviation was calculated as:

$$Deviation\ (\%) = \left(\frac{I - I_{ens}}{I_{ens}}\right) \times 100 \tag{5}$$

Where I is the intensity estimated by a given distribution and I_{ens} is the mean intensity across candidate models. This metric was used to quantify relative model deviation, not as an absolute measure of bias. Upper-tail stability was assessed from the physical consistency of high-return-period estimates across durations.

No single criterion was used in isolation. The preferred distribution was selected based on consistently good fit, low ensemble-relative deviation, and stable upper-tail behaviour across durations and return periods. Full distribution equations, PTIII/LPTIII implementation details, and model-ranking results are provided in Supplementary Text S1 and Supplementary Table S4.

2.4. Rainfall duration disaggregation, uncertainty assessment, and model integration

Due to the limited availability of long-term sub-daily rainfall observations, short-duration rainfall depths were also derived from daily AMS using the empirical disaggregation method adopted by GMet (2016):

$$R_T = \left(\frac{T_d}{24}\left(\frac{24+B}{T_d+B}\right)^n\right)R_{24} \tag{6}$$

Where R_T is the rainfall depth at duration T_d, and R_{24} is the 24-hour rainfall depth, B and n are empirical regional parameters. The method was applied to durations of 12, 24, and 42 min, and 1, 2, 3, 4, 5, 6, 12, and 24 h.

To quantify uncertainty associated with the empirical scaling, B and n were varied around their baseline values using $B = 0.6 \pm 0.1$ and $n = 0.96 \pm 0.05$. For each parameter combination, IDF curves were recomputed for the five daily rainfall stations: Airport, KNUST, Kwadaso, Bekwai, and Owabi. Uncertainty was summarized using percentage deviation from the baseline estimate and uncertainty envelopes across durations and return periods. Variance analysis shows that the parameter n contributes more to overall uncertainty than B, confirming the dominant role of the nonlinear scaling exponent in uncertainty propagation. Although this framework improves robustness, a few limitations remain. Extreme value estimates rely on statistical extrapolation beyond observed records, thereby introducing uncertainty at high return periods (Katz et al., 2002). Also, the disaggregation method remains empirical and does not explicitly resolve sub-daily rainfall-generating processes, even though parameter sensitivity is explicitly quantified. Finally, the assumption of stationarity in the AMS is maintained, consistent with classical IDF development practice, but without explicit consideration of climate non-stationarity (Milly et al., 2008). Despite these constraints, the combined framework of estimating and intercomparing IDF curves from AMS of direct sub-daily and disaggregated daily rainfall data provides a transparent and operationally relevant basis for IDF curve development in data-scarce environments that balance statistical rigor with pragmatic reconstruction of sub-daily rainfall behaviour.

2.5. Validation metrics and percentage deviation analysis

Agreement between reference IDF curves (IDF_{der}) obtained from the concatenated sub-daily KMRGN was evaluated using percentage deviation, RMSE, and NSE across durations and return periods. Percentage deviation was calculated as:

$$\%Deviation = \frac{IDF_{der} - IDF_{ref}}{IDF_{ref}} \times 100 \tag{7}$$

where positive values indicate overestimation and negative values indicate underestimation relative to the reference curve. Relative error magnitude was assessed using RMSE:

$$RMSE = \sqrt{\frac{1}{n}\sum_{i=1}^{n}\left(IDF_{der,i} - IDF_{ref,i}\right)^2} \tag{8}$$

.

Overall agreement was further assessed using the Nash-Sutcliffe Efficiency:

$$NSE = 1 - \frac{\sum_{i=1}^{n}\left(IDF_{ref,i} - IDF_{der,i}\right)^2}{\sum_{i=1}^{n}\left(IDF_{ref,i} - \overline{IDF_{ref}}\right)^2} \tag{9}$$

Where $\overline{IDF_{ref}}$ denotes the mean of the IDFs obtained from the KMRGN. Metrics were computed across all durations for each return period. In addition, inter-station and inter-duration variability were used to describe the spread of IDF estimates and provide uncertainty envelopes around the reference curves.

3. Results and discussions

3.1. Model intercomparison and sensitivity analysis

The four candidate distributions: GEV, Gumbel, PTIII, and LPTIII were evaluated using goodness-of-fit statistics, ensemble-relative

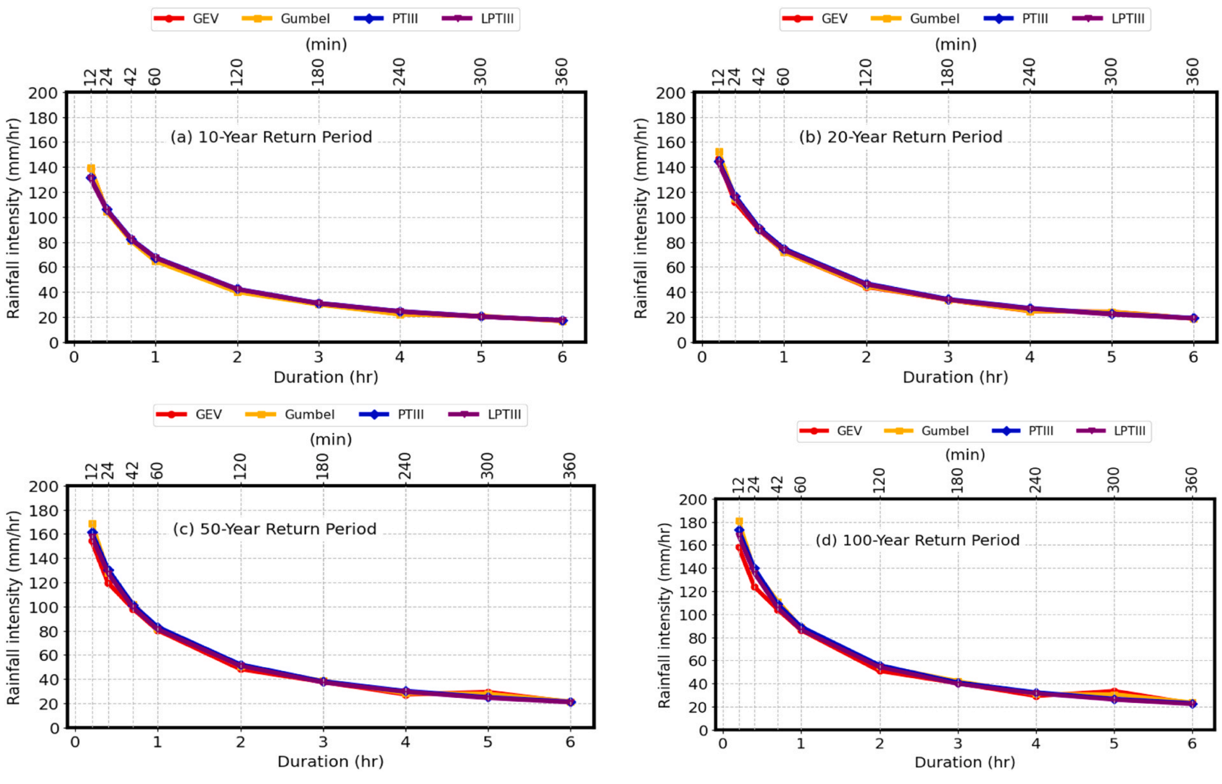

Fig. 4. Intercomparison of IDF curves derived from the GEV (red), Gumbel (yellow), PTIII (blue), and LPTIII (magenta) distributions for return periods of (a) 10, (b) 20, (c) 50, and (d) 100 years, based on the concatenated sub-daily KMRGN dataset.

deviation, and distributional behaviour across durations and return periods (Fig. 4). All models produced comparable goodness-of-fit statistics, with only small differences in KS values (0.0959–0.1049) and χ^2 statistics (5.93–6.21). The GEV distribution yielded the lowest KS and χ^2 values, indicating the closest fit to the empirical distribution. However, it also produced the lowest mean rainfall intensity (65.28 mm h^{-1}) and the largest negative deviation from the model ensemble (−1.35%), indicating lower upper-tail estimates relative to the other models.

The Gumbel and PTIII distributions produced higher mean intensities (67.80 and 67.55 mm h^{-1}, respectively) and positive ensemble-relative deviations, forming the upper range of model estimates. In contrast, LPTIII showed near-optimal goodness-of-fit (KS = 0.0968; χ^2 = 5.98) and the smallest ensemble-relative deviation (−0.58%). Fig. 4 confirms this behaviour: model curves remain closely clustered at lower return periods but diverge at 50–100 years, especially at shorter durations, where differences in upper-tail behaviour become more pronounced.

Based on the combined evidence, LPTIII was selected as the preferred distribution for IDF estimation because it provides a balanced compromise between goodness-of-fit, ensemble-relative deviation, and upper-tail stability. Gumbel and PTIII may be interpreted as more conservative upper-range estimates, whereas GEV gives lower high-return-period estimates. The expected near-linear behaviour of the IDF curves in log-log space is provided in Supplementary Figure S1.

3.2. *Concatenated sub-daily KMRGN stations versus individual sub-daily KMRGN stations*

The regional representativeness of the concatenated KMRGN series was assessed by comparing its IDF curves with those derived from individual sub-daily stations. Although several stations cover 8–9 calendar years, the strict ≥ 90% completeness criterion reduces the number of valid years per station to a maximum of five. Therefore, individual stations with at least two valid years were compared against the concatenated KMRGN series, which contains 36 station-years (Fig. 5a-d).

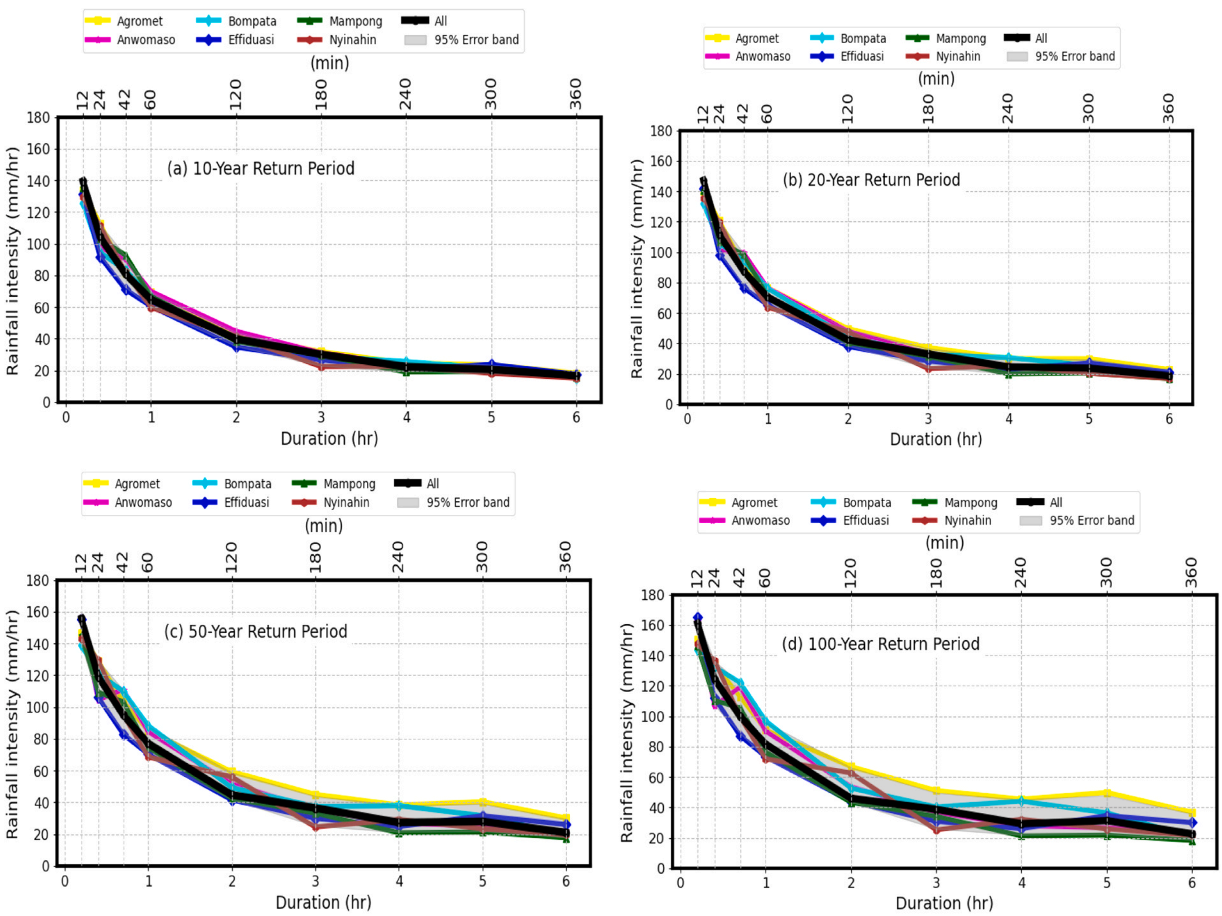

Fig. 5. IDF curves obtained from the concatenated sub-daily KMRGN stations (All; black curve) and individual sub-daily stations across the analyzed return periods, including Agromet (yellow), Anwomaso (magenta), Bompata (cyan), Effiduasi (blue), Mampong (green), and Nyinahin (brown). The spread among station curves relative to the concatenated reference series represents the empirical inter-station variability and associated uncertainty in regional rainfall representation, with greater divergence observed at short durations due to convective-scale heterogeneity and progressively stronger convergence at intermediate and long durations, reflecting increasing spatial uniformity of rainfall intensities.

Using the concatenated KMRGN series as a reference, performance metrics indicate generally strong agreement, although station-dependent variability remains. Across return periods, NSE values range from 0.90 to 0.99, RMSE from approximately 4.2–14.4 mm h^{-1} , and PBIAS from about −9.0% to +16.4%. The concatenated IDF curves are generally positioned near the center of the individual station estimates, indicating that the pooled series captures the regional rainfall structure while reducing the influence of station-specific anomalies.

The largest deviations occur at short durations, particularly below 1 h, where convective rainfall is highly localized. At longer durations, especially from about 2–6 h, individual station curves converge toward the concatenated series, with reduced deviations and improved NSE values. This pattern indicates that local convective variability dominates short-duration extremes, whereas longer-duration rainfall is more spatially coherent across the network.

Overall, the concatenated KMRGN series provides a suitable regional reference for IDF estimation. However, it should not be interpreted as replacing site-specific extremes. Rather, it offers a statistically more stable regional estimate, while individual station curves remain important for assessing localized high-intensity rainfall behaviour.

3.3. Concatenated sub-daily KMRGN stations versus results from disaggregated individual daily GMet stations

The disaggregated daily rainfall series was evaluated against the concatenated sub-daily KMRGN IDF curves to assess whether long-term daily data can provide an operational alternative where continuous sub-daily observations are unavailable. IDF curves from the disaggregated daily stations are compared with the concatenated KMRGN reference in Fig. 6, while summary performance metrics are provided in Table 1. Detailed duration- and station-level deviations are provided in Supplementary Table S5.

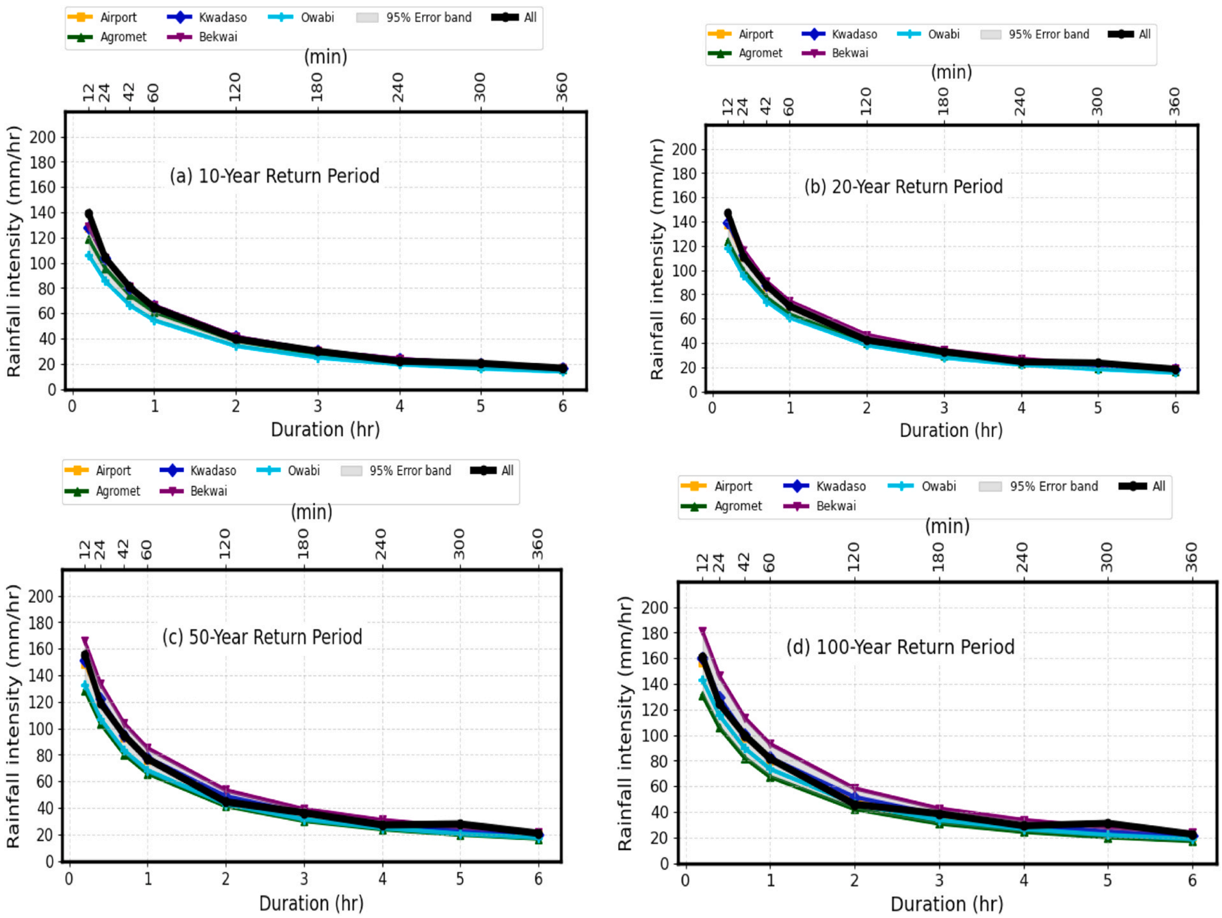

Fig. 6. IDF curves obtained from the concatenated sub-daily KMRGN stations (All) and the results from the daily GMet disaggregation across the given return periods. The concatenated KMRGN (black curve), Kumasi Airport (yellow curve), Agromet (green curve), Kwadaso (blue curve), Bekwai (purple), and Owabi (cyan curve) are shown for comparison. The shaded region represents the empirical 95% uncertainty band, defined by the deviation between the sub-daily reference series and the disaggregated station-based estimates at each duration. The band highlights scale-dependent uncertainty introduced by the disaggregation process, with wider dispersion at short-duration extremes and selected high return periods, and progressively reduced divergence at intermediate and long durations, indicating increasing convergence between the datasets for long-duration rainfall characteristics.

Table 1
Performance evaluation metrics of disaggregated station IDF curves relative to concatenated sub-daily KMRGN (*All*)(ref) averaged/(aggregated for RMSE) across durations for each return period.

Station	Return Period (Years)	RMSE	PBIAS (%)	NSE	MD
Airport	10	3.967	−1.861	0.99	−1.072
Airport	20	3.488	−1.993	0.993	−1.236
Airport	50	3.136	−1.836	0.995	−1.232
Airport	100	3.369	−1.575	0.995	−1.11
Agromet	10	7.843	−8.741	0.963	−5.034
Agromet	20	9.818	−11.742	0.947	−7.284
Agromet	50	12.689	−15.343	0.92	−10.295
Agromet	100	14.95	−17.828	0.896	−12.573
Kwadaso	10	3.81	−1.477	0.991	−0.851
Kwadaso	20	3.047	−0.883	0.995	−0.548
Kwadaso	50	2.762	−0.078	0.996	−0.053
Kwadaso	100	3.413	+ 0.518	0.995	+ 0.365
Bekwai	10	3.64	−1.018	0.992	−0.586
Bekwai	20	3.277	+ 3.298	0.994	+ 2.046
Bekwai	50	7.834	+ 9.092	0.97	+ 6.101
Bekwai	100	12.452	+ 13.541	0.928	+ 9.549
Owabi	10	14.336	−18.561	0.875	−10.69
Owabi	20	12.614	−15.61	0.913	−9.683
Owabi	50	10.351	−12.357	0.947	−8.292
Owabi	100	8.793	−10.25	0.964	−7.229

Overall, the disaggregated daily estimates show moderate to strong agreement with the sub-daily reference, although performance varies by station and duration. Across stations and return periods, NSE ranges from 0.875 to 0.996, RMSE from 2.76 to 14.95 mm h^{-1} , and PBIAS from −18.56% to +13.54%. Airport and Kwadaso show the closest agreement, with low RMSE values and NSE values close to 1.0. In contrast, Owabi and Agromet show larger deviations, indicating stronger local sensitivity to the disaggregation procedure.

The largest discrepancies occur at short durations, particularly between 12 and 42 min, where disaggregated estimates generally underestimate the observed sub-daily reference. This behaviour is consistent with the smoothing of short-duration convective rainfall peaks when daily totals are redistributed to sub-daily durations. At intermediate durations, especially between about 42 min and 6 h, deviations generally decrease, and the disaggregated curves align more closely with the concatenated KMRGN reference. At longer durations, agreement improves for some stations, although station-dependent biases persist.

The empirical inter-station uncertainty envelope indicates that uncertainty is strongly duration-dependent, with the widest spread at short durations and selected high-return-period combinations. This suggests the main limitation of the disaggregation approach.

3.4. Concatenated sub-daily KMRGN stations versus concatenated disaggregated daily GMet stations

The regional performance of the disaggregation approach was further assessed by concatenating the disaggregated daily stations into a 220-station-year regional series and comparing it with the concatenated sub-daily KMRGN reference. This comparison evaluates whether regional pooling improves the ability of disaggregated daily data to reproduce the sub-daily IDF structure. The resulting IDF curves are shown in Fig. 7, with duration-specific deviations provided in Table 2.

Overall, the two concatenated series show strong agreement, with NSE values ranging from 0.968 to 0.995, RMSE from 2.99 to 8.21 mm h^{-1} , and PBIAS from −4.35% to +8.25%. This indicates that regional pooling substantially reduces station-specific variability relative to the individual-station comparison. However, deviations remain duration-dependent rather than uniformly small.

At short durations, especially near 12 min, the disaggregated regional series tends to underestimate the sub-daily reference at lower return periods but shifts toward slight overestimation at higher return periods. At intermediate durations, deviations vary, with overestimation most evident around 2–4 h and close agreement around 6–12 h. At 24 h, the disaggregated series tends to underestimate the sub-daily reference, particularly at higher return periods. These patterns indicate that the disaggregation procedure can reproduce the broad regional IDF structure but may redistribute rainfall depth unevenly across durations.

The empirical deviation envelope confirms that uncertainty is duration-dependent, with the largest spread occurring at sub-hourly and selected intermediate durations. Thus, the concatenated disaggregated daily series provides a practical regional alternative where long-term sub-daily observations are unavailable, especially for intermediate durations, but caution remains necessary for very short durations and high return periods.

3.5. Major and minor rainy seasons of the concatenated sub-daily KMRGN versus disaggregated daily GMet data

Rainfall in southern West Africa follows a bimodal regime, with a major rainy season from March to July and a minor rainy season from September to November. Because rainfall organization and convective intensity differ between these seasons, the seasonal performance of the disaggregated daily data was evaluated against the concatenated sub-daily KMRGN reference. The seasonal IDF comparisons are shown in Fig. 8 and Table 3, with detailed deviations provided in Supplementary Tables S6 and S7.

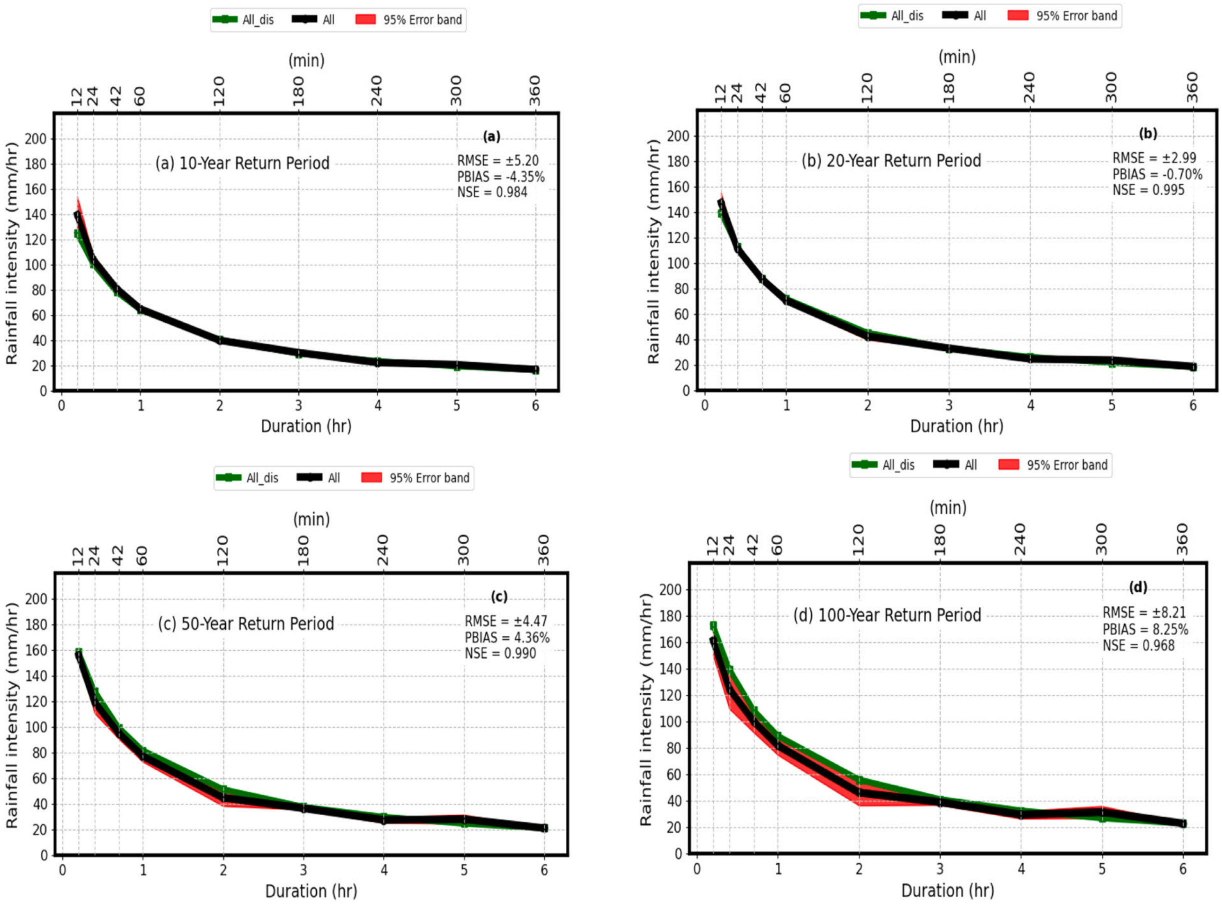

Fig. 7. IDF curves obtained from the concatenated KMRGN stations and the results from the concatenated daily disaggregation from GMet across the given return periods (10, 20, 50, and 100 years). The concatenated KMRGN stations (All, black curve) and the concatenated disaggregated daily AMS (All_dis, green curve) are shown for comparison. The shaded region represents the 95% empirical uncertainty band, defined by the deviation between the two datasets at each duration. The band highlights scale-dependent differences, with greater spread at sub-hourly durations and progressively reduced divergence at longer durations and higher return periods, indicating strong convergence in extreme rainfall behaviour between both datasets.

Table 2
Comparison of IDF values from the concatenated sub-daily KMRGN stations (*All*) (ref) and the concatenated disaggregated daily AMS (Alldis) (derived). The percentage deviations are indicated as (% incr), with (+) and (-) signs showing increasing and decreasing rainfall intensities across the respective storm durations and return periods.

		All_{dis} versus All										
Duration	10-Year			20-Year			50-Year			100-Year		
	All_{dis}	All	**% incr.**	All_{dis}	All	**% incr.**	All_{dis}	All	**% incr.**	All_{dis}	All	**% incr.**
12 mins	124.57	139.38	**−10.62**	139.3	147.25	**−5.4**	158.35	155.71	**+1.7**	172.63	161.07	**+7.18**
24 mins	100.55	104.2	**−3.5**	112.44	111.28	**+1.04**	127.82	119.19	**+7.24**	139.34	124.39	**+12.02**
42 mins	78.16	80.83	**−3.3**	87.4	87.49	**−0.1**	99.36	94.99	**+4.6**	108.32	99.95	**+8.37**
1 hr	64.04	64.7	**−1.02**	71.61	70.38	**+1.74**	81.4	77.03	**+5.67**	88.74	81.6	**+8.76**
2 hrs	40.18	39.81	**+0.92**	44.93	42.24	**+6.36**	51.08	44.61	**+14.49**	55.68	45.97	**+21.14**
3 hrs	29.4	30.08	**−2.27**	32.87	32.98	**−0.31**	37.37	36.36	**+2.79**	40.74	38.68	**+5.34**
4 hrs	23.24	22.19	**+4.71**	25.98	24.46	**+6.2**	29.54	27.24	**+8.44**	32.2	29.22	**+10.21**
5 hrs	19.24	20.52	**−6.27**	21.51	23.67	**−9.11**	24.45	27.91	**−12.39**	26.66	31.24	**−14.67**
6 hrs	16.43	16.64	**−1.23**	18.37	18.54	**−0.9**	20.88	20.89	**−0.02**	22.77	22.59	**+0.81**
12 hrs	8.83	8.83	**+0.02**	9.88	9.92	**−0.48**	11.23	11.31	**−0.71**	12.24	12.33	**−0.73**
24 hrs	4.65	4.71	**−1.36**	5.2	5.43	**−4.33**	5.91	6.41	**−7.91**	6.44	7.19	**−10.47**

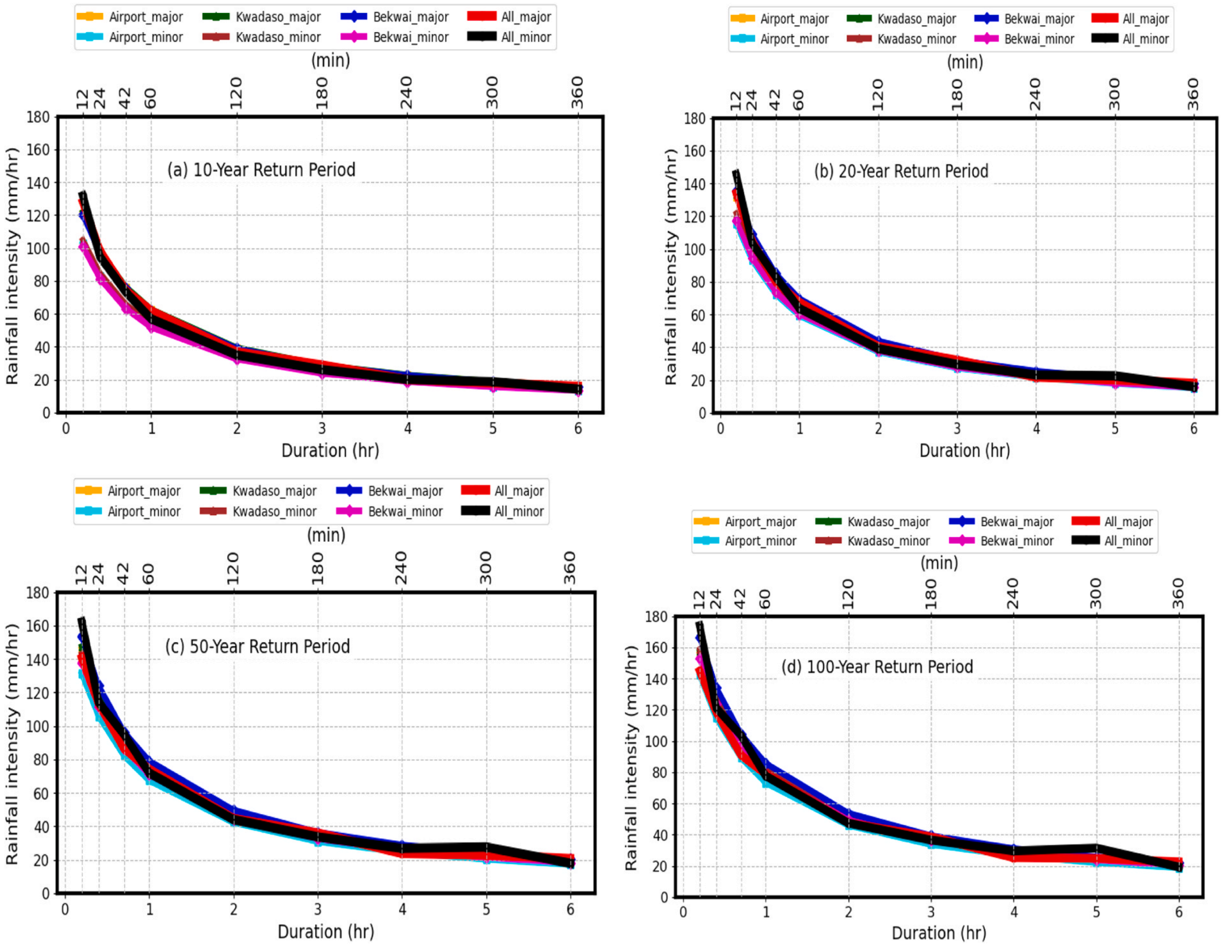

Fig. 8. IDF curves obtained from the major and minor rainy seasons for the concatenated sub-daily KMRGN stations and the disaggregated daily AMS from GMet stations across the given return periods. Major rainy season for the concatenated KMRGN (red curve), minor rainy season for concatenated DACCIWA (red curve), major rainy season for disaggregated AMS at Kumasi (yellow curve), minor rainy season for disaggregated AMS at Kumasi (cyan curve), major rainy season for disaggregated AMS at Kwadaso (darkgreen curve), minor rainy season for disaggregated AMS at Kwadaso (brown curve), major rainy season for disaggregated AMS at Bekwai (blue curve), and minor rainy season for disaggregated AMS at Bekwai (magenta).

During the major rainy season, disaggregated daily data reproduce the sub-daily reference reasonably well beyond the shortest durations. At 12 min, underestimation is evident but station-dependent, while deviations generally narrow at intermediate and longer durations. Across representative stations, most deviations remain within approximately ±10%, although larger departures occur at selected durations and return periods. This indicates that the disaggregation procedure captures the broader major-season rainfall structure but still smooths short-duration intensity peaks.

In contrast, the minor rainy season shows larger and more systematic underestimation, particularly at sub-hourly durations. At 12 min, disaggregated estimates are typically about 20–24% lower than the sub-daily reference across stations and return periods. Deviations decrease with increasing duration, but negative biases persist through intermediate durations before partial convergence at 12–24 h. This pattern indicates that daily accumulation-based disaggregation is less able to reproduce the short-lived convective bursts that dominate minor-season extremes.

Overall, the seasonal analysis shows that disaggregation uncertainty is not uniform throughout the year. It is strongest during the minor rainy season and at the shortest durations, where convective intermittency and peak rainfall intensity are most poorly represented by daily data. Seasonal correction factors or season-specific disaggregation parameters may therefore be required for reliable short-duration IDF estimation.

3.6. Existing GMet IDF curves versus results from the disaggregated individual daily GMet stations

The updated disaggregated daily IDF estimates were compared with the existing GMet 2016 IDF curves for Kumasi, Kwadaso, and Bekwai to assess how design rainfall estimates change when the daily AMS is extended to 2023 using a comparable disaggregation

Table 3
Performance evaluation metrics of the disaggregated station IDF curves relative to concatenated sub-daily KMRGN (*All*)(ref) averaged/(aggregated for RMSE) across durations for each return period.

Station	Return Period (years)	RMSE	PBIAS (%)	NSE	MD
Concatenated KMRGN versus Disaggregated Stations for the major rainy season					
Airport	10	2.671	−0.143	0.995	−0.077
Airport	20	1.809	+1.416	0.998	+0.816
Airport	50	3.334	+3.428	0.993	+2.14
Airport	100	5.312	+4.894	0.984	+3.216
Kwadaso	10	2.501	+0.655	0.996	+0.35
Kwadaso	20	2.096	+2.362	0.997	+1.362
Kwadaso	50	4.016	+4.449	0.99	+2.778
Kwadaso	100	6.05	+5.921	0.98	+3.89
Bekwai	10	2.826	−0.661	0.994	−0.353
Bekwai	20	2.804	+3.84	0.995	+2.213
Bekwai	50	7.155	+8.852	0.97	+5.527
Bekwai	100	10.768	+12.164	0.935	+7.993
Concatenated KMRGN versus Disaggregated Stations for the minor rainy season					
Station	**Return Period (years)**	**RMSE**	**PBIAS (%)**	**NSE**	**MD**
Airport	10	11.063	−13.201	0.917	−6.902
Airport	20	11.439	−12.609	0.926	−7.368
Airport	50	11.935	−11.964	0.934	−7.881
Airport	100	12.348	−11.549	0.937	−8.216
Kwadaso	10	9.992	−11.309	0.932	−5.912
Kwadaso	20	8.597	−7.971	0.958	−4.658
Kwadaso	50	6.981	−4.050	0.977	−2.668
Kwadaso	100	6.457	−1.374	0.983	−0.977
Bekwai	10	11.956	−14.749	0.902	−7.711
Bekwai	20	10.558	−11.213	0.937	−6.552
Bekwai	50	8.868	−7.384	0.963	−4.864
Bekwai	100	7.943	−4.920	0.974	−3.50

approach. The comparison is shown in Fig. 9, with detailed duration- and return-period-specific deviations provided in Supplementary Tables S8 and S9.

The updated curves generally exceed the 2016 GMet curves across durations and return periods, although the magnitude of the difference varies by station. Kumasi and Bekwai show moderate increases, typically around 7–10%, whereas Kwadaso shows substantially larger deviations, exceeding 40–50% at higher return periods. These differences indicate that updated data and processing can materially affect design rainfall estimates.

However, the increases should not be interpreted as definitive evidence of climatic intensification. Trend and change-point tests applied to the extended AMS indicate no statistically significant monotonic trends or structural breaks across the analyzed stations. The differences relative to the 2016 curves are therefore more plausibly attributed to the longer sampling period, differences in record structure or quality, and sensitivity of the disaggregation procedure, rather than confirmed non-stationary behaviour in rainfall extremes.

The large deviations at Kwadaso appear station-specific and should be interpreted cautiously. They may reflect local data characteristics or the sensitivity of the disaggregation method to station-level rainfall variability. Overall, the comparison highlights the need to periodically update operational IDF curves, while distinguishing updated design estimates from formal evidence of climate-driven changes in extremes.

4. Conclusion

This study developed regional IDF relationships for Ghana's Ashanti Region using high-resolution sub-daily rainfall observations from the KMRGN. Thirteen stations satisfying strict completeness and quality-control criteria were concatenated into a 36-station-year regional series. L-moment regional frequency analysis supported the statistical homogeneity of the selected network, while Mann-Kendall and change-point tests showed no statistically significant trends or structural breaks in the AMS. These results support the use of a stationary regional frequency-analysis framework for the available record.

Extreme rainfall quantiles were estimated using a multi-model framework comparing GEV, Gumbel, Pearson Type III, and Log-Pearson Type III distributions. Although all candidate distributions provided acceptable fits, the Log-Pearson Type III distribution offered the most balanced performance in terms of goodness-of-fit, ensemble-relative deviation, and upper-tail stability. The concatenated sub-daily KMRGN series therefore provides a robust regional benchmark for evaluating IDF estimates derived from alternative data sources.

The main findings are as follows:

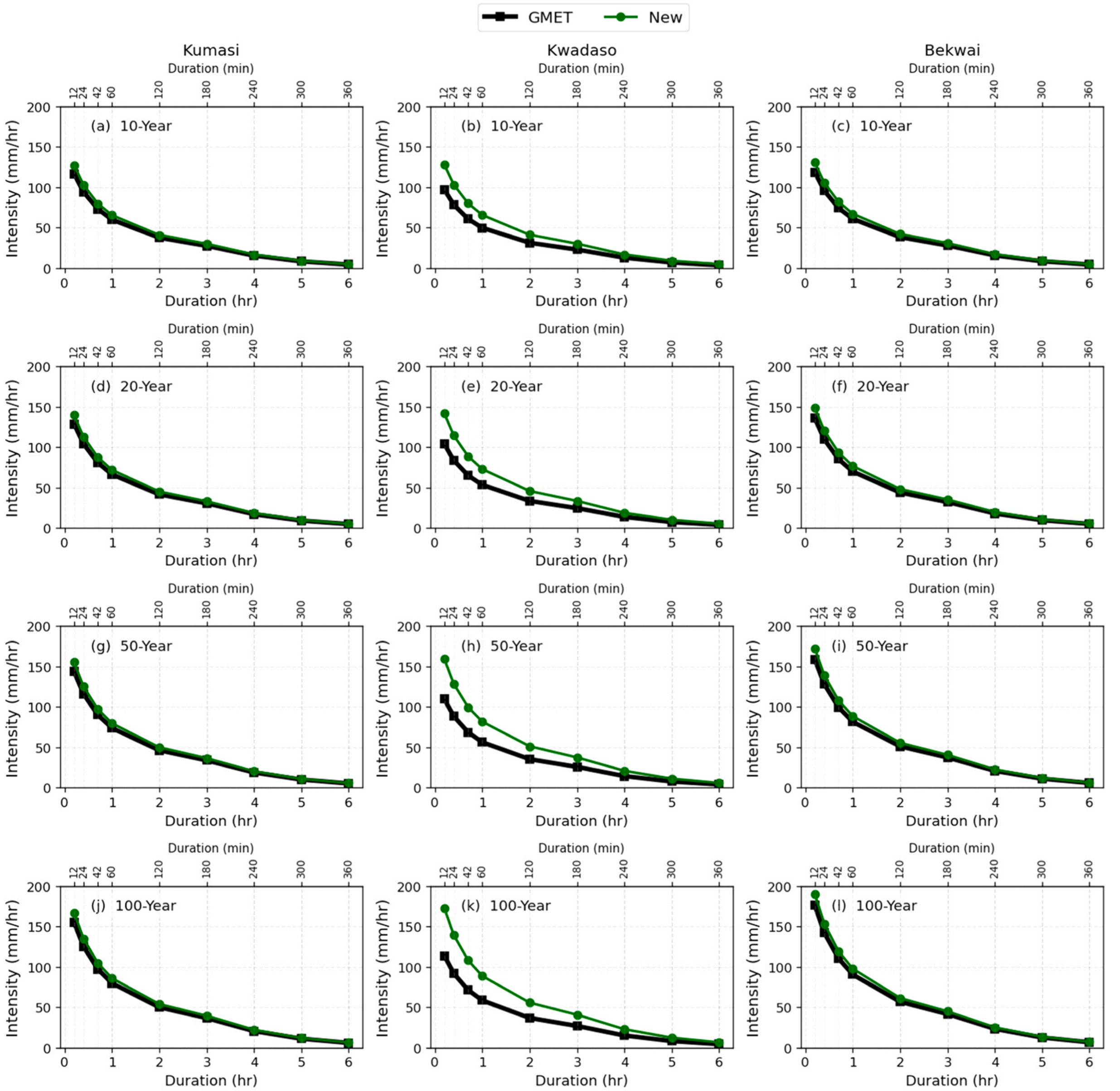

Fig. 9. Graphical comparison of IDF curves derived from the disaggregated daily station data (green) and the existing GMet IDF curves (black) for the selected return periods. Kumasi is denoted by letters (a), (d), (g), and (j); Kwadaso is denoted by (b), (e), (h), and (k), and Bekwai is denoted by (c), (f), (i), and (l).

- **Concatenated sub-daily data provide the most reliable regional IDF reference.** The concatenated sub-daily KMRGN series captures the regional structure of short-duration rainfall extremes while reducing the influence of station-specific anomalies. It is therefore suitable as a regional IDF reference, although individual station records remain important for site-specific design.
- **Disaggregated daily data are unreliable at short durations but adequate at longer durations:** Disaggregated daily data reproduce the general IDF structure but underestimate short-duration intensities, particularly below 1 h, by up to about 18%. Agreement improves at intermediate and longer durations, indicating that daily-based disaggregation better preserves cumulative rainfall structure than sub-daily peak intensities.
- **Concatenating disaggregated daily stations restores regional representativeness:** When disaggregated daily stations are **concatenated** into a 220 station-year regional series, agreement with the sub-daily KMRGN reference improves substantially, with high NSE values and relatively low bias. This suggests that concatenated disaggregated daily data can provide a practical regional alternative where long-term sub-daily observations are unavailable, but caution is required at very short durations and high return periods.

- **Seasonality significantly influences disaggregation accuracy:** Seasonal analysis shows that disaggregation performance is strongly season-dependent. The minor rainy season exhibits a larger underestimation of short-duration extremes, approximately 19–24%, reflecting the difficulty of reconstructing short-lived convective bursts from daily totals. Season-specific correction methods may therefore be needed for reliable short-duration IDF estimation.
- **Rainfall intensities have intensified since GMet's 2016 update:** Updated IDF estimates for Kumasi, Kwadaso, and Bekwai exceed the existing 2016 GMet curves across several durations and return periods. However, because **the** AMS trend and change-point tests do not indicate statistically significant non-stationarity, these differences should not be interpreted as definitive evidence of climate-driven intensification. They are more plausibly associated with extended sampling, data-processing differences, and methodological sensitivity.

The progressive reduction in percentage differences with increasing duration demonstrates that daily disaggregation preserves cumulative rainfall totals more effectively than sub-daily peak variability, a limitation widely noted in stochastic and scaling-based disaggregation approaches (Haacke and Paton, 2021). Station-specific contrasts further indicate that localized convective characteristics influence how extremes are reconstructed from daily data, consistent with findings that IDF relationships in tropical regions are highly sensitive to storm-type composition and mesoscale organization (Klein et al., 2021; Shusse et al., 2015). The marked seasonal asymmetry suggests that short-lived, high-intensity rainfall typical of the minor rainy season is particularly susceptible to smoothing during temporal redistribution, whereas the more organized rainfall systems of the major season yield comparatively smaller biases. This behaviour aligns with evidence that warm-rain-dominated convective systems produce sharp intensity peaks that are poorly represented when daily totals are uniformly redistributed (Hamada et al., 2015).

In relation to previous IDF assessments in Ghana, this study advances the methodological framework by constructing a high-resolution regional reference through the concatenation of sub-daily stations rather than relying solely on individual station analyses or temporally disaggregated daily records. The integration of regional homogeneity testing, temporal consistency analysis, multi-model intercomparison, and uncertainty quantification represents a more comprehensive and statistically rigorous framework for IDF development in data-scarce regions. While earlier curve updates provided important regional benchmarks (e.g., Arhin-Acquah, 2016; Abubakari et al., 2017), the present analysis quantifies the magnitude and duration-dependence of disaggregation bias and demonstrates its strong seasonal modulation. This clarifies why daily-based IDF curves may perform unevenly in convectively dominated tropical environments, where rainfall variability is governed by both thermodynamic moisture availability and mesoscale dynamical processes (Klein et al., 2021; Yoshida, 2021).

The systematic positive deviations relative to the 2016 curves further indicate a regional intensification of rainfall extremes over the past decade, consistent with thermodynamic amplification expected under warming conditions following the Clausius-Clapeyron relationship (Westra et al., 2014; Rahmstorf, 2024). The near-uniform increases observed across durations imply that both short-duration convective processes and longer-duration rainfall systems, including MCSs, have strengthened (Shusse et al., 2015; Yoshida, 2021). Nevertheless, the statistical stationarity of the AMS suggests that these changes remain within the bounds of natural variability over the period of record, reinforcing the appropriateness of a stationary modeling framework for current design applications. Extending the curves to 2023 reveals trends that were not yet evident in earlier assessments and underscores the importance of periodic IDF updates in rapidly changing climatic conditions. These findings establish the concatenated sub-daily series as the most robust regional benchmark, while validating the concatenated disaggregated daily series as a practical alternative in data-scarce environments (regions). The results emphasize the need for continued investment in dense gauge networks, sub-hourly monitoring, and seasonally informed correction methodologies to support reliable flood-risk assessment and climate-resilient infrastructure planning (Haacke and Paton, 2021).

CRediT authorship contribution statement

G.A. Torsah: Conceptualization, Methodology, Formal analysis, Investigation, Data Curation, Writing – Original Draft, Visualization, Project Administration. **M. Maranan:** Validation, Software, Writing – Review & Editing, Project Administration. **V. Akyeampong:** Validation, Writing – Review & Editing. **K.A. Adjei:** Resources, Funding acquisition, Writing – Review & Editing, Supervision. **L.K. Amekudzi:** Resources, Funding acquisition, Writing – Review & Editing, Supervision. **A.H. Fink:** Conceptualization, Funding acquisition, Resources, Writing – Review & Editing, Supervision.

Declaration of Competing Interest

The authors declare that they have no known competing financial interests or personal relationships that could have appeared to influence the work reported in this paper.

Acknowledgement

The authors acknowledge funding from the German Federal Ministry of Education and Research (BMBF) through the WASCAL Research Action Plan 2.0 (WRAP2.0) FURIFLOOD project (Current and future risks of urban and rural flooding in West Africa-An integrated analysis and eco-system-based solutions (KNUST; 01LG1001A; KIT: 01LG2086A). The second and last authors also receive funding from the BMBF/BMFTR project German Academic Network for Capacity Development in Climate Change Adaptations in Africa (NetCDA; Grants 01LG2301E, 01LG2601E). Finally, we thank the anonymous reviewers for their thoughtful and constructive comments, which have significantly improved the manuscript.

Appendix A. Supporting information

Supplementary data associated with this article can be found in the online version at doi:10.1016/j.ejrh.2026.103718.

Data availability

Data will be made available on request.

References

Abubakari, S., Kusi, K.A., Xiaohua, D., 2017. Revision of the rainfall intensity duration frequency curves for the city of Kumasi (Ghana). Int. J. Eng. Sci. 6, 51–56.
Adjei-Mensah, K., Kusimi, J.M., 2020. Dwindling water supply and its socio-economic impact in sekyere kumawu district in ashanti region of ghana: public opinion on the role of climate change. GeoJournal 85, 1355–1372.
Ageet, S., Fink, A.H., Maranan, M., Diem, J.E., Hartter, J., Ssali, A.L., Ayabagabo, P., 2022. Validation of satellite rainfall estimates over equatorial east africa. J. Hydrometeorol. 23, 129–151.
Agyekum, J., Amekudzi, L.K., Stein, T., Aryee, J.N., Atiah, W.A., Adefisan, E.A., Danuor, S.K., 2023. Verification of satellite and model products against a dense rain gauge network for a severe flooding event in kumasi, ghana. Meteorol. Appl. 30, e2150.
Amekudzi, L.K., Yamba, E.I., Preko, K., Asare, E.O., Aryee, J., Baidu, M., Codjoe, S.N., 2015. Variabilities in rainfall onset, cessation and length of rainy season for the various agro-ecological zones of ghana. Climate 3, 416–434.
Amekudzi, L.K., Osei, M.A., Atiah, W.A., Aryee, J.N., Ahiataku, M.A., Quansah, E., Preko, K., Danuor, S.K., Fink, A.H., et al., 2016. Validation of trmm and fews satellite rainfall estimates with rain gauge measurement over ashanti region, Ghana. Atmos. Clim. Sci. 6, 500.
Amoateng, P., Finlayson, C.M., Howard, J., Wilson, B., 2018. A multi-faceted analysis of annual flood incidences in kumasi, Ghana. Int. J. Disaster risk Reduct. 27, 105–117.
Ansah, S., Ahiataku, M., Yorke, C., Otu-Larbi, F., Yahaya, B., Lamptey, P., Tanu, M., 2020. Meteorological analysis of floods in Ghana. Adv. Meteorol. 2020, 1–14.
Arhin-Acquah, R., 2016. Review of the hydraulic capacity of some existing culverts on selected roads in Kumasi Metropolis. Ph.D. thesis. KNUST, Ghana.
Asante-Annor, A., Oti, D., 2019. Rainstorm intensity-duration-frequency model for Tarkwa, ghana. Ghana. Min. J. 19, 21–28.
Asibey, M.O., Agyeman, K.O., Amponsah, O., Ansah, T., 2020. Patterns of land use, crop and forest cover change in the Ashanti region, Ghana. J. Sustain. For. 39, 35–60.
Asubonteng, K.O., Andah, E.I., 2001. Characterization and evaluation of inland valley watersheds for sustainable agricultural production: Case study of semi-deciduous forest zone in the Ashanti region of Ghana. Tropics 10, 539–553.
Campion, B.B., Venzke, J.F., 2013. Rainfall variability, floods and adaptations of the urban poor to flooding in kumasi, ghana. Nat. Hazards 65, 1895–1911.
Cannon, A.J., Innocenti, S., 2019. Projected intensification of sub-daily and daily rainfall extremes in convection-permitting climate model simulations over North America: Implications for future intensity-duration-frequency curves. Nat. Hazards Earth Syst. Sci. 19 (2), 421–440.
Chow, V.T., 1988. Freq. Anal. 392.
Claude, N.J., Lin, S., Fabrice, N., Twagirayezu, G., Khan, J., Marnn, P., Yousef, A.A.A.A.M., Dawuda, U.K., Bazel, M.A.A.S., Hussein, A.Aa., et al., 2021. Establishment of rainfall intensity-duration-frequency equations and curves used to design an appropriate and sustainable hydraulic structure for controlling flood in nyabugogo catchment-rwanda.
Coles, S., Bawa, J., Trenner, L., Dorazio, P., 2001. An introduction to statistical modeling of extreme values, 208. Springer.
Dankwa, J.B., 1974. Maximum rainfall intensity-duration frequencies in Ghana (Republic of Ghana). Meteorol. Serv. Dep.
Estrany-Planas, P., Blanco-Gómez, P., Ortiz-Vallespí, J.I., Orihuela-Martínez, J., Vilarrasa, V., 2025. Regional Frequency Analysis Using L-Moments for Determining Daily Rainfall Probability Distribution Function and Estimating the Annual Wastewater Discharges, 12. Hydrology, p. 152.
Fordjour, A., Anyemedu, F., Adjei, O., Ajani, A., Zhu, X., 2019. Development of intensity-duration frequency curves for koforidua city in ghana. Eur. Sci. J. 15, 83–84.
Ghana Meteorological Agency, GMet, 2016. Consultancy services for the coordination of the review of the intensity-duration-frequency (idf) of the rainfall intensity graph over ghana, Unpublished manuscript, 2024. Ministry of Roads and Highways, Ghana Meteorological Agency. Department of History, Harvard University, Accra.
Gumbel, E.J., 1958. Statistics of extremes. Columbia university press.
Haacke, N., Paton, E.N., 2021. Analysis of diurnal, seasonal, and annual distribution of urban sub-hourly to hourly rainfall extremes in germany. Hydrol. Res. 52, 478–491.
Hamada, A., Takayabu, Y.N., Liu, C., Zipser, E.J., 2015. Weak linkage between the heaviest rainfall and tallest storms. Nat. Commun. 6, 6213.
Hosking, J.R., Wallis, J.R., 1997. Reg. Freq. Anal. (New York).
Katz, R.W., Parlange, M.B., Naveau, P., 2002. Statistics of extremes in hydrology. Adv. Water Resour. 25 (8–12), 1287–1304.
Klein, C., Nkrumah, F., Taylor, C.M., Adefisan, E.A., 2021. Seasonality and trends of drivers of mesoscale convective systems in southern west africa. J. Clim. 34, 71–87.
Koutsoyiannis, D., 2004. Statistics of extremes and estimation of extreme rainfall: II. Empirical investigation of long rainfall records/Statistiques de valeurs extrêmes et estimation de précipitations extrêmes: II. Recherche empirique sur de longues séries de précipitations. Hydrol. Sci. J. 49 (4).
Leadbetter, M.R., 1974. On extreme values in stationary sequences. Z. F. üR. Wahrscheinlichkeitstheorie Verwandte. Geb. 28, 289–303.
Maranan, M., Fink, A.H., Knippertz, P., 2018. Rainfall types over southern west africa: Objective identification, climatology and synoptic environment. Q. J. R. Meteorol. Soc. 144, 1628–1648.
Maranan, M., Fink, A.H., Knippertz, P., Amekudzi, L.K., Atiah, W.A., Stengel, M., 2020. A process-based validation of gpm imerg and its sources using a mesoscale rain gauge network in the west african forest zone. J. Hydrometeorol. 21, 729–749.
Mensah, N.O., Twintoh, J.J., Amrago, E.C., Donkor, A., Anang, S.A., 2021. Forestry insurance preference among tree growers in the ashanti region of ghana: a tobit and multi-nomial regression approach. Manag. Finance.
Milly, P.C., Betancourt, J., Falkenmark, M., Hirsch, R.M., Kundzewicz, Z.W., Lettenmaier, D.P., Stouffer, R.J., 2008. Stationarity is dead: Whither water management? Science 319 (5863), 573–574.
Nicholson, S.E., 2013. The West African Sahel: A review of recent studies on the rainfall regime and its interannual variability. Int. Sch. Res. Not. 2013 (1), 453521.
Niemczynowicz, J., 1999. Urban hydrology and water management-present and future challenges. Urban. Water 1, 1–14.
Olsson, J., 1998. Evaluation of a scaling cascade model for temporal rain-fall disaggregation. Hydrol. earth Syst. Sci. 2 (1), 19–30.
Osei, M.A., Amekudzi, L.K., Omari-Sasu, A.Y., Yamba, E.I., Quansah, E., Aryee, J.N., Preko, K., 2021. Estimation of the return periods of maxima rainfall and floods at the pra river catchment, ghana, west africa using the gumbel extreme value theory. Heliyon 7.
Panthou, G., Vischel, T., Lebel, T., Blanchet, J., Quantin, G., Ali, A., 2012. Extreme rainfall in west africa: A regional modeling. Water Resour. Res. 48.
Owusu-Ansah, J.K., 2016. The influences of land use and sanitation infrastructure on flooding in kumasi, ghana. GeoJournal 81, 555–570.

Panthou, G., Vischel, T., Lebel, T., 2014. Recent trends in the regime of extreme rainfall in the central sahel. Int. J. Climatol. 34, 3998–4006.

Pickands III, J., 1975. Statistical inference using extreme order statistics. the Annals of Statistics, 119-131.

Rahmstorf, S., 2024. Climate and weather at 3 ° more: Earth as we don't (want to) know it, in. 3 ° More: The Impending Hot Season and How Nature Can Help Us Prevent It. Springer, pp. 3–17.

Sam, M., Nwaogazie, I., Ikebude, C., 2021. Improving indian meteorological department method for 24-hourly rainfall downscaling to shorter durations for idf modeling. Int. J. Hydrol. 5, 72–82.

Shusse, Y., Maki, M., Shimizu, S., Iwanami, K., Maesaka, T., Suzuki, S.I., Sakurai, N., Misumi, R., 2015. Relationship between precipitation core behaviour in cumulonimbus clouds and surface rainfall intensity on 18 august 2011 in the kanto region, japan. J. Meteorol. Soc. Jpn. Ser. II 93, 215–228.

Torsah, G.A., Osei, M.A., Aryee, J., Oti, J.A., Amekudzi, L.K., 2025. Triggers of inland heavy rainfall inducing convective storms in west africa: Case study of june, 2021. Weather. Clim. Extrem. 47, 100740.

Westra, S., Fowler, H.J., Evans, J.P., Alexander, L.V., Berg, P., Johnson, F., Kendon, E.J., Lenderink, G., Roberts, N., 2014. Future changes to the intensity and frequency of short-duration extreme rainfall. Rev. Geophys. 52, 522–555.

Yoshida, S., 2021. Study on short-term forecast of localized heavy rainfall based on the statistical characteristics of cumulonimbus clouds observed by Ka-band doppler radars.